

Joint Antenna Position and Beamforming Optimization with Self-Interference Mitigation in MA-ISAC System

Size Peng*, Cixiao Zhang*, Yin Xu, Qingqing Wu, Xiaowu Ou and Dazhi He

Cooperative Medianet Innovation Center (CMIC), Shanghai Jiao Tong University, Shanghai 200240, China

Email: {sjtu2019psz, cixiaozhang, xuyin, qingqingwu, xiaowu_ou, hedazhi}@sjtu.edu.cn

Abstract—Movable antennas (MAs) have demonstrated significant potential in enhancing the performance of integrated sensing and communication (ISAC) systems. However, the application in the integrated and cost-effective full-duplex (FD) monostatic systems remains underexplored. To address this research gap, we develop an MA-ISAC model within a monostatic framework, where the self-interference channel is modeled in the near field and characterized by antenna position vectors. This model allows us to investigate the use of MAs with the goal of maximizing the weighted sum of communication capacity and sensing mutual information. The resulting optimization problem is non-convex making it challenging to solve optimally. To overcome this, we employ fractional programming (FP) to propose an alternating optimization (AO) algorithm that jointly optimizes the beamforming and antenna positions for both transceivers. Specifically, closed-form solutions for the transmit and receive beamforming matrices are derived using the Karush–Kuhn–Tucker (KKT) conditions, and a novel coarse-to-fine grained search (CFGS) approach is employed to determine the high-quality sub-optimal antenna positions. Numerical results demonstrate that with strong self-interference cancellation (SIC) capabilities, MAs significantly enhance the overall performance and reliability of the ISAC system when utilizing our proposed algorithm, compared to conventional fixed-position antenna designs.

Index Terms—Movable antenna, integrated sensing and communication, monostatic full-duplex system, self-interference cancellation, joint transceiver optimization, coarse-to-fine-grained searching (CFGS).

I. INTRODUCTION

The increasing demand for reliable sensing and efficient communication has sparked significant interest in Integrated Sensing and Communication (ISAC) technologies. ISAC aims to merge communication and sensing functions within a single system, utilizing the same frequency bands and hardware resources. This integration optimizes spectral resource utilization, reduces hardware costs, and simplifies system complexity, positioning ISAC as a highly promising and efficient approach for modern wireless networks. Recent studies [1]–[3] indicate that ISAC systems can achieve notable improvements in spectral efficiency compared to traditional systems that separate these functions. As wireless networks advance towards 6G and beyond, ISAC is expected to play a crucial

role in meeting the growing demands for higher data rates, lower latency, and improved connectivity.

Beamforming design is critical in both multiple-input multiple-output (MIMO) communication and sensing systems due to its precoding capabilities. However, traditional systems with fixed, equally spaced antennas cannot fully exploit the spatial degrees of freedom (DOF) offered by the antennas. To address this limitation, a movable antenna (MA) system, also known as a fluid antenna system, has been proposed. This system can adjust antenna spacing using flexible RF chains, capturing the spatial variations of wireless channels. This approach has proven effectiveness in enhancing MIMO performance by jointly optimizing the precoding matrix and the positions of the transmit antenna, as demonstrated in [4].

The full-duplex (FD) monostatic ISAC setup is particularly appealing for automotive and IoT applications due to its seamless integration, cost-effectiveness, and efficient use of the spectrum [5]. Although some existing studies have explored the use of MAs in the ISAC scenario [6]–[8], a full-duplex (FD) monostatic scenario remains under-researched. This paper pioneers the investigation of the effectiveness of movable antennas in this important and challenging setup. In particular, self-interference cancellation (SIC) is a critical issue under this setup. High performance can only be achieved with strong SIC capability. Unlike physical isolation methods, active suppression of SI can be achieved through Tx and Rx beamforming [9], [10]. Motivated by [10]–[12], we model the SI channel as a near-field channel and characterize it by the positions of the transmit and receive antennas, allowing for more precise control and reduction of self-interference.

We consider several clutters as sensing interferences in this monostatic FD system. To characterize the trade-off between communication and sensing, we adopt a weighted sum of communication rate and sensing mutual information (MI). The beamforming matrix and antenna positions at Tx and Rx are optimized using the alternating optimization (AO) method. Specifically, we propose a coarse-to-fine grained searching (CFGS) algorithm to determine a high-quality sub-optimal antenna positions. Our contributions are threefold

- We model FD monostatic MA-ISAC system, including the SI channel characterized by antenna position vectors

*These authors contributed equally to this work.
The corresponding author is Yin Xu (e-mail: xuyin@sjtu.edu.cn).

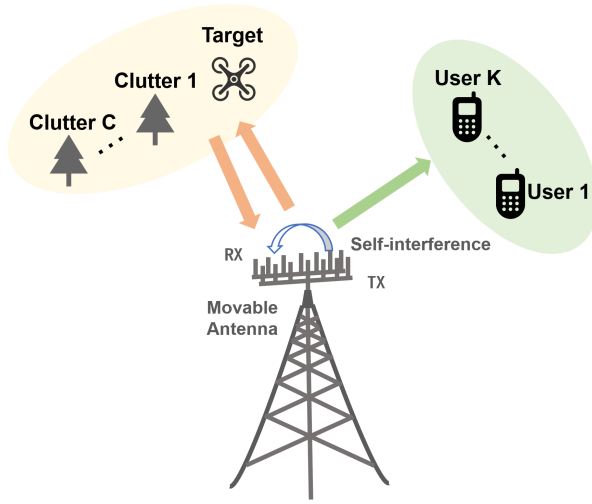


Fig. 1. System model of the monostatic MA-ISAC system.

of the transmitter and receiver. This enables the strategic positioning of the MA to mitigate interference.

- We propose a method to jointly optimize the transmit and receive beamforming matrices along with the Tx/Rx antenna positions.
- Numerical results demonstrate the effectiveness of our algorithm in enhancing performance in a monostatic FD ISAC system.

Notations: $\mathbf{x}(n)$, \mathbf{x}^T , \mathbf{x}^* , $\text{Tr}(\mathbf{X})$, and $(\mathbf{X})^{-1}$ denote the n th entry of \mathbf{x} , the transpose of \mathbf{x} , the conjugate of \mathbf{x} , the trace of \mathbf{X} and the inverse of \mathbf{X} , respectively.

II. SYSTEM MODEL

In this paper, we consider a monostatic FD base station (BS) with N_T linear Tx-MA and N_R linear Rx-MA surrounded by K users, C clutters and a sensing target, as illustrated in Fig. 1. The antenna positions in Tx and Rx can move flexibly within the region $[X_{\min}, X_{\max}]$ and $[Y_{\min}, Y_{\max}]$, respectively.

A. Channel model

The antenna positions of Tx and Rx are denoted as $\mathbf{x} = [x_1, \dots, x_{N_T}]^T$ and $\mathbf{y} = [y_1, \dots, y_{N_R}]^T$. According to the far-field response model in [13], the transmit steering vector of Tx is

$$\mathbf{a}_{k,l}(\mathbf{x}) = [1 \quad e^{j\frac{2\pi}{\lambda}x_1 \cos(\theta_{k,l})} \quad \dots \quad e^{j\frac{2\pi}{\lambda}x_{N_T} \cos(\theta_{k,l})}]^T \in \mathbb{C}^{N_T}, \quad (1)$$

where $\theta_{k,l}$ denotes the angle of departure of l^{th} path of k^{th} user. Assume η_k is the free space fading factor and $\rho_{k,l}$ is the channel gain coefficient experienced by the l^{th} path of the k^{th} user. Therefore, the channel between the BS and the k^{th} user is

$$\mathbf{h}_k(\mathbf{x}) = \frac{\eta_k}{\sqrt{L_p}} \sum_{l=1}^{L_p} \rho_{k,l} \mathbf{a}_{k,l}(\mathbf{x}) \in \mathbb{C}^{N_T}. \quad (2)$$

Additionally, the receive steering vector for sensing is

$$\mathbf{b}(\mathbf{y}) = [1 \quad e^{j\frac{2\pi}{\lambda}y_1 \cos(\psi)} \quad \dots \quad e^{j\frac{2\pi}{\lambda}y_{N_R} \cos(\psi)}]^T \in \mathbb{C}^{N_R}, \quad (3)$$

Therefore, the channel for sensing is

$$\mathbf{h}_s(\mathbf{x}, \mathbf{y}) = \frac{\eta_s}{\sqrt{L_p}} \sum_{l=1}^{L_p} \rho_s \mathbf{a}_s(\mathbf{x}) \mathbf{b}_s^H(\mathbf{y}) \in \mathbb{C}^{N_T \times N_R}. \quad (4)$$

As the array apertures at the transceiver and the operating frequency increase (leading to a decrease in the wavelength λ), the distance between the transceivers becomes less than the MIMO Rayleigh distance of $\frac{(D_T + D_R)^2}{\lambda}$ [11]. Consequently, different from the far-field channel, the SI channel should be modeled as a near-field channel [10], [12], [14]. We define $r(x_i, y_j)$ as the distance between the i^{th} transmit antenna and the j^{th} receive antenna, where r_0 represents the distance between X_{\min} and Y_{\min} , as demonstrated in Fig. 2. This distance can be expressed as

$$r(x_i, y_j) = \sqrt{r_0^2 + x_i^2 + y_j^2 + 2r_0 y_j \sin(\theta) - 2r_0 x_i \sin \theta - 2x_i y_j} \quad (5)$$

Thus, the self-interference channel model can be modeled as

$$\mathbf{H}_{\text{SI}}(\mathbf{x}, \mathbf{y}) = \left(\eta_{\text{SI}} e^{-j\frac{2\pi}{\lambda} r_{x_i, y_j}} \right)_{N_T \times N_R}, \quad (6)$$

where

$$\eta_{\text{SI}} = \frac{G_l}{4} \left[\left(\frac{\lambda}{2\pi r_{x_i, y_j}} \right)^2 - \left(\frac{\lambda}{2\pi r_{x_i, y_j}} \right)^4 + \left(\frac{\lambda}{2\pi r_{x_i, y_j}} \right)^6 \right]_{N_T \times N_R} \quad (7)$$

denotes the free space fading factor.

B. Signal model

Let $\mathbf{s} = [s_1, s_2, \dots, s_K]$, $\mathbb{E}\{\mathbf{s}\mathbf{s}^H\} = \mathbf{I}$ denotes the signals for K users, which is used for both communication and sensing. The transmit and receive beamforming matrices are

$$\mathbf{F} = [\mathbf{f}_1, \mathbf{f}_2, \dots, \mathbf{f}_K] \in \mathbb{C}^{N_T \times K}, \quad (8)$$

$$\mathbf{W} = [\mathbf{w}_1, \mathbf{w}_2, \dots, \mathbf{w}_{N_R}]^H \in \mathbb{C}^{N_R}. \quad (9)$$

Thus, the baseband received signal at k^{th} user is

$$r_k = \mathbf{h}_k^H(x) \mathbf{f}_k s_k + \mathbf{h}_k^H \sum_{j=1, j \neq k}^K \mathbf{f}_j s_j + n_k. \quad (10)$$

We can derive

$$\text{SINR}_k = \frac{|\mathbf{h}_k^H(x) \mathbf{f}_k|^2}{\sum_{j=1, j \neq k}^K |\mathbf{h}_k^H(x) \mathbf{f}_j|^2 + \sigma_k^2}. \quad (11)$$

Thus,

$$R_k = \log(1 + \text{SINR}_k). \quad (12)$$

Received signal at BS with receive beamforming is

$$\begin{aligned} r_s &= \alpha_s \mathbf{w}^H \mathbf{b}_s(\mathbf{y}) \mathbf{a}_s^H(\mathbf{x}) \mathbf{F} \mathbf{s} + \sum_{c=1}^C \mathbf{w}^H (\alpha_c \mathbf{b}_c(\mathbf{y}) \mathbf{a}_c^H(\mathbf{x}) \mathbf{F} \mathbf{s}) \\ &\quad + \mathbf{w}^H \mathbf{H}_{\text{SI}}(\mathbf{x}, \mathbf{y}) \mathbf{F} \mathbf{s} + \mathbf{w}^H \mathbf{n}_s. \end{aligned} \quad (13)$$

Thus, we can get

$$\text{SCNR}_s = \frac{|\alpha_s \mathbf{w}^H \mathbf{b}_s(\mathbf{y}) \mathbf{a}_s^H(\mathbf{x}) \mathbf{F}|^2}{\sum_{c=1}^C |\alpha_c \mathbf{w}^H \mathbf{b}_c(\mathbf{y}) \mathbf{a}_c^H(\mathbf{x}) \mathbf{F}|^2 + |\mathbf{w}^H \mathbf{H}_{\text{SI}}(\mathbf{x}, \mathbf{y}) \mathbf{F}|^2 + \sigma_s^2}. \quad (14)$$

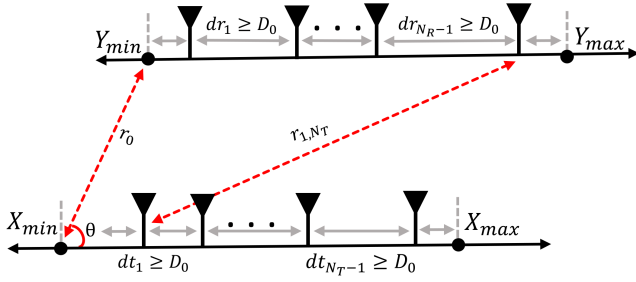


Fig. 2. Movable antenna model at Tx and Rx.

Following the approach in [6], [15], sensing MI can be expressed as

$$R_s = \log(1 + \text{SINR}_s). \quad (15)$$

C. Problem formulation

To balance the communication and sensing performance, we aim to maximize the weighted sum of communication rate and sensing MI in (12) and (15). Hence, the optimization problem is formulated as

$$(P1) \max_{\mathbf{F}, \mathbf{x}, \mathbf{y}, \mathbf{w}} \mathcal{G}(\mathbf{F}, \mathbf{x}, \mathbf{y}, \mathbf{w}) = \varpi_c \sum_{k=1}^K R_k + \varpi_s R_s \quad (16a)$$

$$\text{s.t. } \text{Tr}(\mathbf{F}^H \mathbf{F}) \leq P_0, \quad (16b)$$

$$\mathbb{E}\{\mathbf{ss}^H\} = \mathbf{I}, \quad (16c)$$

$$X_{\min} \leq \mathbf{x} \leq X_{\max}, Y_{\min} \leq \mathbf{y} \leq Y_{\max}, \quad (16d)$$

$$|x_i - x_j| \geq D_0, |y_j - y_j| \geq D_0, \forall i, \hat{i}, j, \hat{j}, i \neq \hat{i}, j \neq \hat{j}, \quad (16e)$$

where P_0 is the maximum transmit power and D_0 is a minimum separation distance between each pair of antennas at the transmitter-receiver for avoiding the coupling effect. The weighted factors ϖ_c and ϖ_s satisfy $\varpi_c + \varpi_s = 1$.

III. PROPOSED SOLUTION

It is challenging to solve (P1) directly because the optimization target (16a) is non-convex with respect to \mathbf{F} , \mathbf{w} , \mathbf{x} , and \mathbf{y} . To address this problem, we employ the fractional programming (FP) approach [16]. Auxiliary variables, including $\boldsymbol{\mu} = [\mu_1, \mu_2, \dots, \mu_K]^T$, $\boldsymbol{\xi}^c = [\xi_1^c, \xi_2^c, \dots, \xi_K^c]^T$, and $\boldsymbol{\xi}^s = [\xi_1^s, \xi_2^s, \dots, \xi_K^s]^T$, are introduced to transform the optimization target in (16a) into an equivalent convex form (25). Subsequently, we propose an alternating optimization (AO) algorithm where the antenna positions, tranciever's beamforming matrices, and auxiliary variables are updated alternately while keeping the others fixed until convergence is achieved.

A. Transmit and Receive Beamforming Optimization

We aim to optimize the transmit and receive beamforming matrix \mathbf{F} and \mathbf{w} with fixed \mathbf{x} , \mathbf{y} and auxiliary variables. Firstly, we formulate the subproblem for \mathbf{F}

$$(SP.1) \max_{\mathbf{F}} \hat{\mathcal{G}}(\mathbf{F}|\mathbf{x}, \mathbf{y}, \mathbf{w}, \boldsymbol{\mu}, \boldsymbol{\xi}^c, \boldsymbol{\xi}^s) \text{ s.t. (16b)}. \quad (17)$$

Since $\hat{\mathcal{G}}$ is a convex function with respect to \mathbf{F} , we can employ the Lagrange dual method to obtain the closed-form expression of \mathbf{F} . The Lagrangian function is defined

as $\mathcal{L}(\mathbf{F}, \lambda) = -\hat{\mathcal{G}}(\mathbf{F}|\mathbf{x}, \mathbf{y}, \mathbf{w}, \boldsymbol{\mu}, \boldsymbol{\xi}^c, \boldsymbol{\xi}^s) + \lambda (\text{Tr}(\mathbf{F}^H \mathbf{F}) - P_0)$. The Lagrangian dual problem is then characterized by the following conditions

$$\frac{\partial \mathcal{L}(\mathbf{F}, \lambda)}{\partial \mathbf{F}} = 0, \quad (18a)$$

$$\text{Tr}(\mathbf{F}^H \mathbf{F}) - P_0 \leq 0, \quad (18b)$$

$$\lambda \geq 0, \quad (18c)$$

$$\lambda (\text{Tr}(\mathbf{F}^H \mathbf{F}) - P_0) = 0. \quad (18d)$$

The closed-form expression of \mathbf{F} can be obtained by solving (18a), which is

$$f_k(\lambda) = \left((\Lambda_k^T + \lambda \mathbf{I})^{-1} \right)^* \varphi_k, \quad (19)$$

where

$$\Lambda_k = \varpi_s \|\boldsymbol{\xi}^s\|^2 \left\{ |\alpha_s|^2 (\mathbf{w}^H \mathbf{b}_s(\mathbf{y}) \mathbf{a}_s^H(\mathbf{x}))^H (\mathbf{w}^H \mathbf{b}_s(\mathbf{y}) \mathbf{a}_s^H(\mathbf{x})) + \sum_{c=1}^C |\alpha_c|^2 (\mathbf{w}^H \mathbf{b}_c(\mathbf{y}) \mathbf{a}_c^H(\mathbf{x}))^H (\mathbf{w}^H \mathbf{b}_c(\mathbf{y}) \mathbf{a}_c^H(\mathbf{x})) + (\mathbf{w}^H H_{\text{SI}}^H(\mathbf{x}, \mathbf{y}))^H (\mathbf{w}^H H_{\text{SI}}^H(\mathbf{x}, \mathbf{y})) + \varpi_c \mathbf{h}_k \mathbf{h}_k^H \right\}, \quad (20)$$

$$\phi_k = \varpi_c \sqrt{1 + \mu_k \xi_k^{c*}} \mathbf{h}_k(\mathbf{x}) + \varpi_s \sqrt{1 + \mu_{K+1} \alpha_s^* \xi_k^{s*}} \mathbf{a}_s(\mathbf{x}) \mathbf{b}_s^H(\mathbf{y}) \mathbf{w}. \quad (21)$$

Similarly, we can derive the closed form of \mathbf{w}

$$\mathbf{w} = \left\{ \{\Psi\}^{-1} \right\}^* \Upsilon, \quad (22)$$

where

$$\Psi = \|\boldsymbol{\xi}^s\|^2 \left\{ \sum_{c=1}^C |\alpha_c|^2 (\mathbf{b}_c(\mathbf{y}) \mathbf{a}_c^H(\mathbf{x}) \mathbf{F}) (\mathbf{b}_c(\mathbf{y}) \mathbf{a}_c^H(\mathbf{x}) \mathbf{F})^H + |\alpha_s|^2 (\mathbf{b}_s(\mathbf{y}) \mathbf{a}_s^H(\mathbf{x}) \mathbf{F}) (\mathbf{b}_s(\mathbf{y}) \mathbf{a}_s^H(\mathbf{x}) \mathbf{F})^H + (H_{\text{SI}}^H(\mathbf{x}, \mathbf{y}) \mathbf{F}) (H_{\text{SI}}^H(\mathbf{x}, \mathbf{y}) \mathbf{F})^H + \sigma_x^2 \mathbf{I} \right\}, \quad (23)$$

$$\Upsilon = \sqrt{1 + \mu_{K+1} \alpha_s} \mathbf{b}_s(\mathbf{y}) \mathbf{a}_s^H(\mathbf{x}) \mathbf{F} \boldsymbol{\xi}^s. \quad (24)$$

To address λ in the complementary slackness condition, we draw inspiration from [6], [17] and employ a bisection method to select an appropriate dual variable.

$$\begin{aligned} \max_{\mathbf{F}, \mathbf{x}, \mathbf{y}, \mathbf{w}, \boldsymbol{\mu}, \boldsymbol{\xi}^c, \boldsymbol{\xi}^s} \hat{\mathcal{G}}(\mathbf{F}, \mathbf{x}, \mathbf{y}, \mathbf{w}, \boldsymbol{\mu}, \boldsymbol{\xi}^c, \boldsymbol{\xi}^s) &= \varpi_c \sum_{k=1}^K \log(1 + \mu_k) + \varpi_s \log(1 + \mu_{K+1}) - \varpi_c \sum_{k=1}^K \mu_k - \varpi_s \mu_{K+1} \\ &+ \varpi_c \sum_{k=1}^K \left[2\sqrt{1 + \mu_k} \text{Re}\{\xi_k^c \mathbf{h}_k^H(\mathbf{x}) \mathbf{f}_k\} - |\xi_k^c|^2 \left(\sum_{j=1}^K |\mathbf{h}_k^H(\mathbf{x}) \mathbf{f}_j|^2 + \sigma_k^2 \right) \right] + \varpi_s \left[2\sqrt{1 + \mu_{K+1}} \text{Re}\{\alpha_s \mathbf{w}^H \mathbf{b}_s(\mathbf{y}) \mathbf{a}_s^H(\mathbf{x}) \mathbf{F} \boldsymbol{\xi}^s\} \right. \\ &\left. - \|\boldsymbol{\xi}^s\|^2 \left(\sum_{c=1}^C \|\alpha_c \mathbf{w}^H \mathbf{b}_c(\mathbf{y}) \mathbf{a}_c^H(\mathbf{x}) \mathbf{F}\|^2 + \|\mathbf{w}^H H_{\text{SI}}^H(\mathbf{x}, \mathbf{y}) \mathbf{F}\|^2 + \|\alpha_s \mathbf{w}^H \mathbf{b}_s(\mathbf{y}) \mathbf{a}_s^H(\mathbf{x}) \mathbf{F}\|^2 + \|\mathbf{w}\|^2 \sigma_s^2 \right) \right]. \quad (25) \end{aligned}$$

B. Auxiliary Variables Optimization

With fixing other parameters, we can update the auxiliary variables ξ^c, ξ^s for quadratic transform parameters by solving the following subproblems

$$(SP.2) \max_{\xi^s, \xi^c} \hat{G}(\xi^s, \xi^c | \mathbf{F}, \mathbf{x}, \mathbf{y}, \mathbf{w}, \mu), \quad (26)$$

Since $\hat{G}(\xi^s, \xi^c | \mathbf{F}, \mathbf{x}, \mathbf{y}, \mathbf{w}, \mu)$ is convex w.r.t. ξ^s and ξ^c , we can obtain the closed-form solutions by setting the partial derivatives of ξ^s and ξ^c to zero, i.e., $\frac{\partial \hat{G}(\xi^s, \xi^c | \mathbf{F}, \mathbf{x}, \mathbf{y}, \mathbf{w}, \mu)}{\partial \xi^c} = 0$ and $\frac{\partial \hat{G}(\xi^s, \xi^c | \mathbf{F}, \mathbf{x}, \mathbf{y}, \mathbf{w}, \mu)}{\partial \xi^s} = 0$. Thus, we can derive the closed-form solution as follows

$$\xi^s = \frac{\sqrt{1 + \mu_{K+1}} (\alpha_s \mathbf{w}^H \mathbf{b}_s(\mathbf{y}) \mathbf{a}_s^H(\mathbf{x}) \mathbf{F})^*}{A}, \quad (27)$$

$$A = \sum_{c=1}^C \|\alpha_c \mathbf{w}^H \mathbf{b}_c(\mathbf{y}) \mathbf{a}_c^H(\mathbf{x}) \mathbf{F}\|^2 + \|\mathbf{w}^H H_{SI}^H(\mathbf{x}, \mathbf{y}) \mathbf{F}\|^2 + \|\alpha_s \mathbf{w}^H \mathbf{b}_s(\mathbf{y}) \mathbf{a}_s^H(\mathbf{x}) \mathbf{F}\|^2 + \|\mathbf{w}\|^2 \sigma_s^2. \quad (28)$$

Similarly, we can derive the closed form of ξ_k^c

$$\xi_k^c = \frac{\sqrt{1 + \mu_{K+1}} \mathbf{f}_k^H \mathbf{h}_k(\mathbf{x})}{\sum_{j=1}^K |\mathbf{h}_k^H(\mathbf{x}) \mathbf{f}_j \mathbf{w}|^2 + \sigma_k^2}. \quad (29)$$

Next should handle the subproblem of μ

$$(SP.3) \max_{\mu} \hat{G}(\mu | \mathbf{F}, \mathbf{x}, \mathbf{y}, \mathbf{w}, \xi^s, \xi^c). \quad (30)$$

This can be easily solved by setting the derivative of μ to zero, which gives

$$\mu_k = \frac{(R_k)^2 + R_k \sqrt{(R_k)^2 + 4}}{2}, k \in \{1, \dots, K+1\}, \quad (31)$$

where $R_k = \text{Re} \{ \xi_k^c \mathbf{h}_k^H(\mathbf{x}) \mathbf{f}_k(\mathbf{x}) \}$, $k = \{1, \dots, K\}$ and $R_{K+1} = \text{Re} \{ \alpha_s \mathbf{w}^H \mathbf{b}_s(\mathbf{y}) \mathbf{a}_s^H(\mathbf{x}) \mathbf{F} \xi_s^s \}$.

Consequently, the algorithm for obtaining the locally optimal solutions of the transceiver beamforming matrices and the introduced auxiliary variables is summarized in **Algorithm 1**.

C. Antenna Positions Optimization

With fixed beamformers, we can update the antenna positions for both \mathbf{x} and \mathbf{y} by solving subproblems

$$(SP.4) \max_{\mathbf{x}} \hat{G}(\mathbf{x} | \mathbf{F}, \mathbf{y}, \mathbf{w}, \mu, \xi^c, \xi^s) \text{ s.t. (16d), (16e)}. \quad (32)$$

$$(SP.5) \max_{\mathbf{y}} \hat{G}(\mathbf{y} | \mathbf{F}, \mathbf{x}, \mathbf{w}, \mu, \xi^c, \xi^s) \text{ s.t. (16d), (16e)}. \quad (33)$$

This problem is difficult to solve directly because of its non-convexity. Thus, we propose a two-stage approach that combines coarse and fine granularity methods for updating antenna positions.

Initially, a coarse search is conducted across grid location sets O_x and O_y to identify appropriate initialization positions. These sets consist of points starting from $x = \mathbf{X}_{\min}$ and $y = \mathbf{Y}_{\min}$ with intervals of λ within the movable range. During this coarse-grained search, N_T points are selected from all

Algorithm 1 Iterative optimization for precoding matrix and received beamforming.

Initialization: Choose the upper bound and lower bound of λ as λ_{\max} and λ_{\min} , tolerance ϵ , power limit P_0 , Randomly initial $\xi_s, \xi_c, \mu, \mathbf{w}$, set iteration index $i=1$.

- 1: **repeat**
- 2: Update $\mathbf{F}^{(i)}$ with the following bisection method
- 3: **repeat**
- 4: Compute $\lambda = (\lambda_{\max} + \lambda_{\min})/2$
- 5: Update precoding matrix $\mathbf{F}^{(i)}$ as (19)
- 6: Compute power P of precoding matrix $\mathbf{F}^{(i)}$
- 7: **if** $P > P_0$ **then**
- 8: $\lambda_{\min} = \lambda$
- 9: **else**
- 10: $\lambda_{\max} = \lambda$
- 11: **end if**
- 12: **until** $|P - P_0| < \epsilon$
- 13: Update $\mathbf{w}^{(i)}, \xi_c^{(i)}, \xi_s^{(i)}, \mu^{(i)}$ as (22), (29), (27), (31) separately
- 14: Update iteration index $i = i + 1$
- 15: **until** the value of (25) converge

Output: $\mathbf{F}^*, \mathbf{w}^*$

possible subsets of O_x , and the objective function is evaluated after the parameters in **Algorithm 1** converge for one iteration. After evaluating all possible combinations, the set yielding the highest objective function value is selected as the initial x . A similar approach is used to select the initial y .

Subsequently, fine-grained adjustments on the best initial points are made using the gradient projection method [4], [6]. The antenna positions $x_n, n \in \{1, \dots, N_T\}$, $y_m, m \in \{1, \dots, N_R\}$ can be alternatively optimized as

$$x_n^{(i+1)} = x_n^{(i)} + \delta^t \nabla_{x_n} \hat{G}(\mathbf{x} | \mathbf{F}, \mathbf{y}, \mathbf{w}, \mu, \xi^c, \xi^s), \quad (34)$$

$$y_m^{(i+1)} = y_m^{(i)} + \delta^t \nabla_{y_m} \hat{G}(\mathbf{y} | \mathbf{F}, \mathbf{x}, \mathbf{w}, \mu, \xi^c, \xi^s), \quad (35)$$

where i denotes the iteration number for antenna inter-loop and δ^t denotes the step size of the gradient descent method. Next, we use projection to meet (16d), (16e). The update process for the receive antenna positions is analogous to that of transmitter. For simplicity, the explanation will focus solely on the transmit antenna positions. We rearrange the antenna indices, i.e. $\mathbf{X}_{\min} \leq \hat{x}_1 \leq \hat{x}_2 \leq \dots \leq \hat{x}_{N_T} \leq \mathbf{X}_{\max}$. The final step involves projecting onto the feasible region, which entails sorting the updated values of \mathbf{x} after the last round of gradient descent in ascending order, reassigning antenna indices accordingly, and then adjusting the antenna spacing. The locally optimal antenna positions can be determined after the projection as follows

$$\begin{cases} \hat{x}_1^{t+1} = \max(\mathbf{X}_{\min}, \min(\mathbf{X}_{\max} - (N-1)D_0, \hat{x}_1^{t+1})), \\ \hat{x}_2^{t+1} = \max(\hat{x}_1^{t+1} + D_0, \min(\mathbf{X}_{\max} - (N-2)D_0, \hat{x}_2^{t+1})), \\ \dots \\ \hat{x}_N^{t+1} = \max(\hat{x}_{N-1}^{t+1} + D_0, \min(\mathbf{X}_{\max}, \hat{x}_N^{t+1})). \end{cases} \quad (36)$$

Algorithm 2 Proposed CFGS algorithm for updating the antenna positions at Tx and Rx.

Initialization: Generate all the possible position alignments of transmit antenna as $\{\zeta_{x1}, \zeta_{x2}, \dots, \zeta_{xs_x}\}$ from \mathbf{O}_X . generate all the possible position alignments of receive antenna as $\{\zeta_{y1}, \zeta_{y2}, \dots, \zeta_{ys_y}\}$ from \mathbf{O}_Y , set iteration index $l = 1$.

- 1: **for** $i = 1, 2, \dots, s_x$ **do**
- 2: **for** $j = 1, 2, \dots, s_y$ **do**
- 3: Let $\mathbf{x} = \zeta_{xi}$, $\mathbf{y} = \zeta_{yj}$
- 4: Converge $\mathbf{F}^{(ij)}$ and $\mathbf{w}^{(ij)}$ with algorithm 1
- 5: Compute $R_{ij} = \mathcal{G}(\mathbf{F}^{(ij)}, \mathbf{x}, \mathbf{y}, \mathbf{w}^{(ij)})$
- 6: **end for**
- 7: **end for**
- 8: Let $\mathbf{x}^{(0)} = \zeta_{xk}$, $\mathbf{y}^{(0)} = \zeta_{yt}$, $k, t = \arg \max R_{kt}$
- 9: **repeat**
- 10: Converge $\mathbf{F}^{(l)}$ and $\mathbf{w}^{(l)}$ with algorithm 1
- 11: Converge $\mathbf{x}^{(l)}$ and $\mathbf{y}^{(l)}$ as (34) and (35)
- 12: Adjust $\mathbf{x}^{(l)}$ and $\mathbf{y}^{(l)}$ as (36)
- 13: Update iteration index $l = l + 1$
- 14: **until** the value of (25) converge

Output: \mathbf{x}^* and \mathbf{y}^*

D. Overall Algorithm

Based on the above subproblems, the overall algorithm to solve (P1) is summarized in **Algorithm 2**.

Complexity Analysis: Denoting I_1 as the coarse-grained search number and I_2 as the fine-grained search iteration number, the overall complexity is

$$\mathcal{O}((I_1 + I_2)(N_T^3 + N_T N_R + N_R^2)). \quad (37)$$

IV. SIMULATION RESULTS

Two algorithms, which use the same beamforming updating method proposed in **Algorithm 1** but differ in antenna configuration, are used for comparison, including fixed Position Antenna (FPA) and gradient descent with movable antenna (GD-MA). In the FPA method, the antenna spaces of the transmit and receive antennas are $\lambda/2$. In the GD-MA method, the transmit and receive antennas are initially randomly located in the movable range and directly optimized with the gradient descent method as shown from **Step 13** to **Step 17** in **Algorithm 2**.

We consider far-filed paths $Lp = 13$, user number $K = 4$, and clutter number $C = 3$. Users, the sensing target and clutters are located randomly around BS. The complex coefficients and the complex channel gain follow the standard complex Gaussian distribution, i.e. $\alpha_c, \alpha_s, \rho_s \sim \mathcal{CN}(0, 1)$. The free space fading factors for far-field are all set as $\eta = \left[\frac{\sqrt{G_T \lambda}}{4\pi d}\right]^2$. The movable range of transmit antenna is 1.5 metre which is 12 times wavelength and for receive antenna is 1 metre which is 8 times wavelength. \mathbf{O}_X and \mathbf{O}_Y are sets of points on movable range of transmit and receive antennas spaced by 1 λ . Communication weighting factor ϖ_c and sensing weighting

TABLE I
PARAMETERS OF THE MONO-STATI MA-ISAC SYSTEM

Parameter	Notation	Value
User and clutter angle	θ_u, θ_c	$[0, \pi]$
Number of transmit antenna	N_T	8
Number of receive antenna	N_R	4
Carrier wavelength	λ	0.01 m
Distance between user and BS	$d_{u,b}$	[50m,80m]
Distance between target and BS	$d_{t,b}$	[10m,20m]
Distance between Rx and Tx antenna gain	d_{T_x, R_x}	0.20 m
	G_l	1
Receive noise power	σ_r^2	-60 dBm
Transmit power	P	30dBm

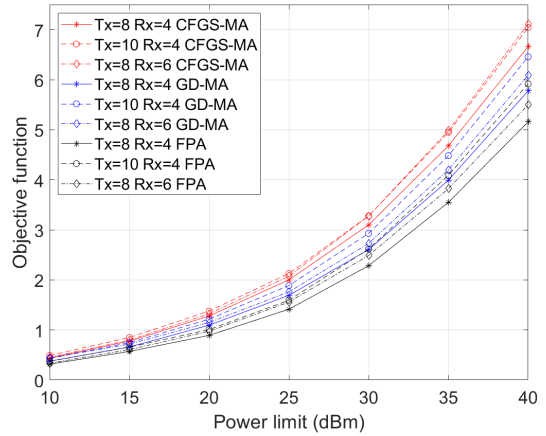


Fig. 3. ISAC performance with different transmit power.

factor ϖ_s are both 0.5. Parameters of the simulation system are shown as **Table I** unless otherwise specified.

Fig. 3 shows the ISAC performance with different transmit power and different number of antennas. The transmit power varies from 10 dBm to 40 dBm, and three sets of antenna numbers are used for simulation, which is 8, 10, 8 for transmit antennas and 4, 4, 6 for receive antennas. The result shows that the objective function grows with increasing transmit power and also with increasing number of transceiver's antennas. When transmit power $P = 30$ dBm, 8 transmit antennas and 4 receive antennas are used. The objective function increases by 14.01% with GD-MA compared to FPA, and a 35.69% increment when CFGS-MA is used compared to FPA. Furthermore, for all three sets of antennas number in the simulation, CFGS-MA shows a better result than GD-MA and FPA.

Fig. 4 shows the ISAC performance with different movable range of transmit and receive antennas. The movable range of transmit antenna varies from 8 to 14 λ , and receive antenna range for 6, 8 and 10 λ . As shown in the result, when GD-MA is used, the result just have a slightly improve since GD-MA can only get a local optimum around the initial position, which can not make full use of the larger movable range. As for CFGS-MA, there is a 13.67% increment of objective function as the movable range of transmit antennas grows from 8 to 14 λ while the movable range of receive antennas is 8 λ . And a 2.81% increment as the movable range of receive antennas

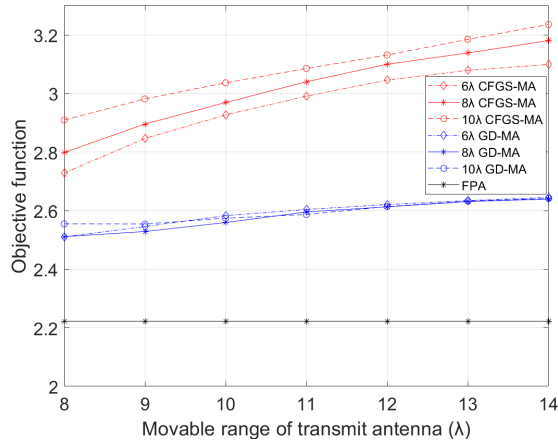


Fig. 4. ISAC performance with different antenna movable range.

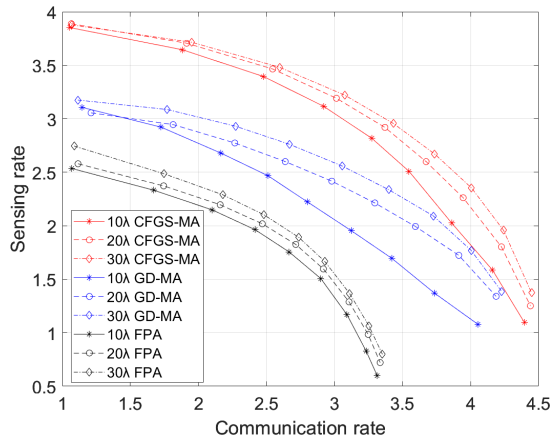


Fig. 5. Trade-off between communication and sensing with different self-interference.

varies from 6 to 10 λ while transmit antennas movable range is 12 λ . The above result shows that CFGS-MA could make good use of movable range.

Fig. 5 shows the trade-off between communication and sensing by varying ϖ_c from 0.1 to 0.9. Additionally, different $d_{Tx,Rx}$ which effects in self interference are compared. The result shows that as the $d_{Tx,Rx}$ become larger, which leading to a lighter self interference, there is a larger rate in most situation. And CFGS-MA could still outperform GD-MA even with greater interference.

V. CONCLUSION

This paper focuses on maximizing the communication rate and mutual information in a monostatic MA-ISAC system. We derive the self-interference channel formula which allows the system to effectively suppress interference. To address the non-convexity of the objective function, we use the FP method to transform the formula. The problem is divided into six subproblems using the AO method. In particular, for the optimization of antenna positions, we compare the proposed CFGS method with the GD-MA and FPA configurations.

Numerical results demonstrate that CFGS offers significant advantages under various conditions.

REFERENCES

- [1] Zhenyao He, Wei Xu, Hong Shen, Derrick Wing Kwan Ng, Yonina C. Eldar, and Xiaohu You, "Full-duplex communication for isac: Joint beamforming and power optimization," *IEEE Journal on Selected Areas in Communications*, vol. 41, no. 9, pp. 2920–2936, 2023.
- [2] Fan Liu, Christos Masouros, Athina P. Petropulu, Hugh Griffiths, and Lajos Hanzo, "Joint radar and communication design: Applications, state-of-the-art, and the road ahead," *IEEE Transactions on Communications*, vol. 68, no. 6, pp. 3834–3862, 2020.
- [3] Fan Liu, Yuanhao Cui, Christos Masouros, Jie Xu, Tony Xiao Han, Yonina C. Eldar, and Stefano Buzzi, "Integrated sensing and communications: Toward dual-functional wireless networks for 6g and beyond," *IEEE Journal on Selected Areas in Communications*, vol. 40, no. 6, pp. 1728–1767, 2022.
- [4] Guojie Hu, Qingqing Wu, Kui Xu, Jiangbo Si, and Naofal Al-Dhahir, "Secure wireless communication via movable-antenna array," *IEEE Signal Processing Letters*, vol. 31, pp. 516–520, 2024.
- [5] J. Andrew Zhang, Md. Lushanur Rahman, Kai Wu, Xiaojing Huang, Y. Jay Guo, Shanzhi Chen, and Jinhong Yuan, "Enabling joint communication and radar sensing in mobile networks—a survey," *IEEE Communications Surveys & Tutorials*, vol. 24, no. 1, pp. 306–345, 2022.
- [6] Wanting Lyu, Songjie Yang, Yue Xiu, Zhongpei Zhang, Chadi Assi, and Chau Yuen, "Flexible beamforming for movable antenna-enabled integrated sensing and communication," *arXiv preprint arXiv:2405.10507*, 2024.
- [7] Chao Wang, Guo Li, Haibin Zhang, Kai-Kit Wong, Zan Li, Derrick Wing Kwan Ng, and Chan-Byoung Chae, "Fluid antenna system liberating multiuser mimo for isac via deep reinforcement learning," *IEEE Transactions on Wireless Communications*, pp. 1–1, 2024.
- [8] Tian Hao, Changxin Shi, Yinghong Guo, Bin Xia, and Feng Yang, "Fluid-antenna enhanced integrated sensing and communication: Joint antenna positioning and beamforming design," *arXiv preprint arXiv:2407.05297*, 2024.
- [9] Kenneth E. Kolodziej, Bradley T. Perry, and Jeffrey S. Herd, "In-band full-duplex technology: Techniques and systems survey," *IEEE Transactions on Microwave Theory and Techniques*, vol. 67, no. 7, pp. 3025–3041, 2019.
- [10] Chengzhe Shi, Wensheng Pan, Ying Shen, and Shihai Shao, "Robust transmit beamforming for self-interference cancellation in star phased array systems," *IEEE Signal Processing Letters*, vol. 29, pp. 2622–2626, 2022.
- [11] Yu Lu and Linglong Dai, "Mixed los/nlos near-field channel estimation for extremely large-scale mimo systems," in *ICC 2023 - IEEE International Conference on Communications*, 2023, pp. 1506–1511.
- [12] Wei Zhang, Ziyu Wen, Cheng Du, Yi Jiang, and Bin Zhou, "Ris-assisted self-interference mitigation for in-band full-duplex transceivers," *IEEE Transactions on Communications*, vol. 71, no. 9, pp. 5444–5454, 2023.
- [13] Lipeng Zhu, Wenyan Ma, and Rui Zhang, "Modeling and performance analysis for movable antenna enabled wireless communications," *IEEE Transactions on Wireless Communications*, vol. 23, no. 6, pp. 6234–6250, 2024.
- [14] Hans Gregory Schantz, "Near field propagation law & a novel fundamental limit to antenna gain versus size," in *2005 IEEE Antennas and Propagation Society International Symposium*. IEEE, 2005, vol. 3, pp. 237–240.
- [15] Zhitong Ni, J. Andrew Zhang, Kai Yang, Xiaojing Huang, and Theodoros A. Tsiftsis, "Multi-metric waveform optimization for multiple-input single-output joint communication and radar sensing," *IEEE Transactions on Communications*, vol. 70, no. 2, pp. 1276–1289, 2022.
- [16] Kaiping Shen and Wei Yu, "Fractional programming for communication systems—part i: Power control and beamforming," *IEEE Transactions on Signal Processing*, vol. 66, no. 10, pp. 2616–2630, 2018.
- [17] Cunhua Pan, Hong Ren, Kezhi Wang, Maged Elkhoshlan, Arumugam Nallanathan, Jiangzhou Wang, and Lajos Hanzo, "Intelligent reflecting surface aided mimo broadcasting for simultaneous wireless information and power transfer," *IEEE Journal on Selected Areas in Communications*, vol. 38, no. 8, pp. 1719–1734, 2020.